Published in final edited form as:

*Free Radic Biol Med*. 2015 October ; 87: 157–168. doi:10.1016/j.freeradbiomed.2015.06.026.

# OKN-007 decreases free radical levels in a preclinical F98 rat glioma model

**Patricia Coutinho de Souza**[a,b], **Nataliya Smith**[a], **Oluwatomisin Atolagbe**[a], **Jadith Ziegler**[a], **Charity Njoku**[a], **Megan Lerner**[c], **Marilyn Ehrenshaft**[d], **Ronald P. Mason**[d], **Bill Meek**[e], **Scott M. Plafker**[f], **Debra Saunders**[a], **Nadezda Mamedova**[a], and **Rheal A. Towner**[a,b,*]

[a]Advanced Magnetic Resonance Center, Oklahoma Medical Research Foundation, 825 NE 13th St., Oklahoma City, OK 73104, USA

[b]Department of Veterinary Pathobiology, College of Veterinary Medicine, Oklahoma State University, Stillwater, OK, USA

[c]Department of Surgery Research Laboratory, University of Oklahoma Health Sciences Center, Oklahoma City, OK, USA

[d]Immunity, Inflammation and Disease Laboratory, National Institute of Environmental Health Sciences, Research Triangle Park, NC, USA

[e]Center for Health Sciences, Oklahoma State University, Tulsa, OK, USA

[f]Free Radical Biology & Aging, Oklahoma Medical Research Foundation, Oklahoma City, OK 73104, USA

## Abstract

Free radicals are associated with glioma tumors. Here, we report on the ability of an anticancer nitrone compound, OKN-007 [Oklahoma Nitrone 007; a disulfonyl derivative of α-phenyl-*tert*-butyl nitrone (PBN)] to decrease free radical levels in F98 rat gliomas using combined molecular magnetic resonance imaging (mMRI) and immunospin-trapping (IST) methodologies. Free radicals are trapped with the spin-trapping agent, 5,5-dimethyl-1-pyrroline *N*-oxide (DMPO), to form DMPO macromolecule radical adducts, and then further tagged by immunospin trapping by an antibody against DMPO adducts. In this study, we combined mMRI with a biotin–Gd-DTPA–albumin-based contrast agent for signal detection with the specificity of an antibody for DMPO nitrone adducts (anti-DMPO probe), to detect *in vivo* free radicals in OKN-007-treated rat F98 gliomas. OKN-007 was found to significantly decrease ($P < 0.05$) free radical levels detected with an anti-DMPO probe in treated animals compared to untreated rats. Immunoelectron microscopy was used with gold-labeled antibiotin to detect the anti-DMPO probe within the plasma membrane of F98 tumor cells from rats administered anti-DMPO *in vivo*. OKN-007 was also found to decrease nuclear factor erythroid 2-related factor 2, inducible nitric oxide synthase, 3-nitrotyrosine, and malondialdehyde in *ex vivo* F98 glioma tissues via immunohistochemistry, as

*Corresponding author at: Advanced Magnetic Resonance Center, Oklahoma Medical Research Foundation, 825 NE 13th St., Oklahoma City, OK 73104, USA. Rheal-Towner@omrf.org (R.A. Towner).

Conflict of interest

The authors declare no competing financial interests.

well as decrease 3-nitrotyrosine and malondialdehyde adducts *in vitro* in F98 cells via ELISA. The results indicate that OKN-007 effectively decreases free radicals associated with glioma tumor growth. Furthermore, this method can potentially be applied toward other types of cancers for the *in vivo* detection of macromolecular free radicals and the assessment of antioxidants.

**Keywords**

Molecular magnetic resonance imaging; Glioma; Free radical; Immuno-spin-trapping; OKN-007; *In vivo*; F98 glioma; Nuclear factor erythroid 2-related factor 2 (Nrf2); Inducible nitric oxide synthase (iNOS); 3-nitrotyrosine (3-NT); Malondialdehyde (MDA)

## 1. Introduction

Free radicals, or more generally, reactive oxygen species (ROS) and reactive nitrogen species (RNS), or collectively RONS, are products of normal cellular metabolism [1], and are formed continuously in cells as a consequence of both enzymatic and nonenzymatic reactions [2]. In normal cells, there is a balance between free radical generation and antioxidant defense [3]. Oxidative damage can occur when this balance is unfavorable, affecting a wide range of molecular species including lipids, proteins, and nucleic acids [4]. Oxidative stress plays a major role in the development of chronic and degenerative diseases such as arthritis, aging, autoimmune disorders, cardiovascular, neurodegenerative diseases, and cancer [5].

By combining molecular magnetic resonance imaging (mMRI) and immunospin-trapping (1ST) technologies it is possible to monitor the levels of free radicals *in vivo* in real time [6]. Free radicals that are generated as a result of oxidative stress processes can be trapped by the spin-trapping compound, 5,5-dimethyl-1-pyrroline *N*-oxide (DMPO), to form DMPO-R adducts (Fig. 1A), which can be further assessed by 1ST, a method that uses an antibody against DMPO–nitrone macromolecule adducts. Therefore, the combined morphologic image resolution of mMRI, the use of a gadolinium (Gd)–DTPA(diethylene triaminepentaacetic acid)–albumin-based contrast agent (Fig. 1B) for signal detection, and the specificity of antibodies for protein/lipid radicals (anti-DMPO antibody, which binds to DMPO–protein/lipid adducts resulting from oxidative stress-induced formation of protein/lipid radicals), can be used to detect *in vivo* oxidative stress-related processes (Fig. 1C) [6,7]. This technique allows *in vivo* assessment of oxidation products, permitting the study of specific cause–consequence relationships from specific oxidative events. Recently our group reported for the first time regarding the use of this noninvasive *in vivo* method to detect and quantify free radical levels in a mouse GL261 glioma model [6].

OKN-007 (2,4-disulfophenyl-PBN; or disodium 4-[(*tert*-butylimino) methyl] benzene-1,3-disulfonate *N*-oxide or disufenton; also previously known as NXY-059) is an anticancer drug [8–10] and free radical spin-trapping agent that inhibits upregulation of inducible nitric oxide synthase (iNOS), decreases glutamate excitotoxicity [11], and has exhibited efficacy as a neuroprotectant. Scientific advancements in our understanding and detection of free radicals in biological systems and their importance in carcinogenesis, as well as the introduction of novel therapeutics such as OKN-007 that act by influencing radicals [8] have

dramatically enhanced our ability to assess the role of free radicals in both disease and normal physiology. In this study, we combined mMRI with a Gd–DTPA–albumin-based contrast agent for signal detection with the specificity of an antibody for DMPO nitrone macromolecule adducts (anti-DMPO probe), to detect *in vivo* free radical levels in untreated and OKN-007-treated adult F98 rat glioma models. As a negative control, we used a nonspecific IgG antibody covalently bound to the albumin–Gd–DTPA-biotin construct. Verification of the presence of the probe in tumor tissues and in glioma cell membranes is also presented.

## 2. Materials and methods

### 2.1. Glioma implantation

The animal studies were conducted with approval from the Institutional Animal Care and Use Committee of the Oklahoma Medical Research Foundation. The F98 rat glioma cell implantation model was prepared as described in our previous work [9]. F98 cells ($10^5$ in 10 μl volume) were intracerebrally implanted with a stereotaxic device (2 mm lateral and 2 mm anterior to the bregma, and at a 3 mm depth) in a total of 15 Fischer 344 rats (male 200–250 g; Harlan Laboratories, Indianapolis, IN). The animals were divided into two groups: OKN-007-treated ($n = 8$) and untreated (UT) ($n = 7$) groups. Both groups were stratified to ensure that tumor sizes were similar before initiation of treatment.

### 2.2. Syntheses of DMPO-specific MRI contrast agents

To recognize the DMPO-radical adducts, we used an anti-mouse/rat monoclonal anti-DMPO antibody bound to a contrast agent. The macromolecular contrast material, biotin–BSA–Gd–DTPA, was prepared using a modification of the method of Dafni et al. [12]. The biotin moiety in the contrast material was added to allow histological localization. Biotin–BSA–Gd–DTPA was synthesized as described in Towner et al. [13]. A solution of biotin–BSA–Gd–DTPA was added directly to the solution of antibody (anti-DMPO, 200 μg/mL) for conjugation through a sulfo-NHS (*N*-succinimidyl-*S*-acetylthioacetate)–EDC (*N*-succinimidyl 3-(2-pyridyldithio)-propionate) link between albumin and antibody according to the protocol of Hermanson [14]. Sulfo-NHS was added to the solution of biotin–BSA–Gd–DTPA and EDC. This activated solution was added directly to the antibody (anti-DMPO, 200 μg/mL) for conjugation. The mixture was left to react for at least 2 h at 25 °C in the dark. The product was lyophilized and subsequently stored at 4 °C and reconstituted to the desired concentration for injections in phosphate buffer saline (PBS). The final amount of the product, anti-DMPO–biotin–BSA–Gd–DTPA (anti-DMPO probe), that was injected into the rats is estimated to be 200 μg anti-DMPO Ab/injection and 100 mg biotin–BSA–Gd–DTPA/injection. The estimated molecular weight of the anti-DMPO–biotin–BSA–Gd–DTPA probe is estimated to be 232 kDa. As negative control, normal rat-IgG conjugated to biotin–BSA–Gd–DTPA (control IgG contrast agent) was synthesized by the same protocol to generate an isotype contrast agent.

### 2.3. DMPO administration

DMPO (ALX-430-090-G001, Enzo Life Sciences) was administered ip (100 mg diluted in 200 μL of saline) 3× daily (every 6 h) for 3 days to trap free radicals during tumor

formation. DMPO administration started when the tumor reached a volume of 70–80 $mm^3$ (Fig. 1D).

### 2.4. OKN-007 treatment

OKN-007 (2,4-disulfophenyl-*N*-*tert*-butyl nitrone, Ryss Laboratories, Union City, CA) was administered as an anticancer agent to the rats in their drinking water at a concentration of 0.018% w/v. The treatment started at 13–15 days after glioma cell implantation, when the tumor volumes were between 10 and 15 $mm^3$ (Fig. 2). The treatment was administered continuously until the end of the study. Rats receiving normal drinking water were used as UT controls. The amount of OKN-007 consumed by each rat, which were housed in separate cages, was determined by weighing water bottles each day. No significant deviation was observed in the volume of liquid uptake of compound in these rats. The average intake of OKN-007 was approximately 10 mg/kg/day. The F98 glioma-bearing rats were divided in three different treatment groups: (1) OKN-007-treated animals + DMPO administration + anti-DMPO probe ($n$=5), (2) untreated animals + DMPO administration + anti-DMPO probe ($n$=7), (3) untreated animals + DMPO administration + IgG probe ($n$=4). The overall experimental scheme is shown in Fig. 1D.

### 2.5. MR Imaging

All MR imaging experiments were conducted on a Bruker Biospec 7.0 T (Bruker Biospin, Germany) using a 72-mm quadrature volume coil for signal transmission and a rat head surface coil for signal reception. Tumor morphology was observed on $T_2$-weighted images obtained with the application of the spin echo pulse sequence, RARE (rapid acquisition with relaxation enhancement) using a TR (repetition time) = 5000 ms, TE (echo time) = 63 ms, 20 transverse 1-mm-thick slices, a field of view of 3.5 × 3.5 $cm^2$ with an in-plane resolution of 137 × 137 × $m^2$. Starting 10 days after the F98 tumor cells inoculation, each rat brain was imaged *in vivo* every 2–3 days until the end of the study. Subsequently for the 3-day DMPO treatment, rats were injected intravenously with anti-DMPO or nonimmune-IgG antibodies tagged with a biotin–Gd–DTPA–albumin-based contrast agent (200 μL/kg; 1 mg antibody/kg; 0.4 mmol $Gd^{+3}$/kg). Rat brains were imaged at 0 (precontrast), 20, 40, 60, 120, and 180 min intervals postprobe or -contrast agent injection.

$T_1$-weighted images were obtained using a variable TR RARE sequence (TR 200, 400, 800, 1200, and 1600 ms; TE 15 ms, FOV 2 × 2 $cm^2$, matrix 256 × 256, slice thickness 0.5 mm, 2 slices, and 2 steps per acquisition).

### 2.6. Calculation of relative probe concentration

Relative probe (contrast agent) concentrations were calculated to assess the levels of macromolecular free radicals in each animal. A contrast difference image was created from the pre- and (120 min) postcontrast datasets for the slice of interest, by computing the difference in signal intensity between the postcontrast and the precontrast image on a pixel basis. On the difference image, three regions of interest (ROI) of equal size (0.02 $cm^2$) were drawn on the areas with the highest $T_1$ relaxation in the tumor parenchyma and contralateral side of the brain of each animal after the probe (anti-DMPO or nonimmune-IgG) injection at the TR 800 ms. The values obtained from the ROIs in the tumor region were normalized to

the contralateral side. The $T_1$ relaxation value of the specified ROIs was computed from all the pixels in the ROI by the following equation [15] (processed by ParaVision 4.0, Bruker): $S(\mathrm{TR}) = S_0(1 - e^{-\mathrm{TR}/\mathrm{T1}})$, where TR is the repetition time, $S_0$ is the signal intensity (integer machine units) at TR $\gg T_1$ and TE = 0, and $T_1$ is the constant of the longitudinal relaxation time. An overlay of the contrast difference image and $T_1$-weighted image was generated using the 3D Analysis Software for Life Sciences Amira (Fei, Hillsboro, OR).

### 2.7. Immunohistochemistry

Whole brains from each rat in each treatment group were removed and embedded in Optimal Cutting Temperature (OCT) compound and frozen in liquid nitrogen. Frozen tissue blocks were sectioned at 10 μm, mounted on positive-charged slides, and air-dried for 10 min. Sections were fixed in cold acetone (−20 °C) for 10 min, dried for 20 min, and incubated with streptavidin–horseradish peroxidase (HRP) polymer kit (Biocare Medical) for 10 min, stained with DAB chromogen (Vector Labs), and then counter-stained with hematoxylin (Vector Labs). The streptavidin binds to the biotin on the anti-DMPO probe if present. For immunohistochemistry (IHC) levels of inducible nitric oxide synthase (iNOS), a rabbit polyclonal anti-rat antibody against iNOS (ab15326; Abcam, Cambridge, MA) was used. For IHC levels of nuclear factor erythroid 2-related factor 2 (Nrf2), a rabbit polyclonal anti-rat antibody against Nrf2 (ab31163; Abcam, Cambridge, MA) was used. For IHC levels of 3-nitrotyrosine (3-NT), a mouse monoclonal antibody against 3-NT (ab61392; Abcam, Cambridge, MA) was used. For IHC levels of malondialdehyde (MDA), a rabbit polyclonal antibody against MDA-PC (protein carrier) (ab6463; Abcam, Cambridge, MA) was used.

### 2.8. Cell treatments with hydrogen peroxide ($H_2O_2$)

F98 cells were cultured in DMEM (Invitrogen, Carlsbad, CA, USA) supplemented with 10% FBS (Invitrogen), and with (or without) 100 μM OKN-007 at 37 °C in a humidified atmosphere containing 5% $CO_2$. The cells were cultured to 70–80% confluence in 25 $cm^2$ flasks. Next, the cells were serum-starved overnight and then treated with $H_2O_2$ (final concentration 50 μM) for a total of 3 h, with a medium change every 30 min. After treatment, the cells were washed with ice-cold PBS (phosphate-buffered saline), and then scraped to collect from culture flasks. The collected cells were incubated on ice in PBS for 20 min, and then centrifuged at 10,000*g* 4 °C for 10 min to remove insoluble materials. The sample protein concentration in the extracts was quantified using a Pierce microplate BSA (bicinchoninic acid) protein assay kit (Pierce Biotechnology, Rockford, IL, USA) using BSA as a standard.

### 2.9. Lipid peroxidation assay

A microplate assay OxiSelect MDA Adduct Competitive ELISA kit (Cell Biolabs, Inc., San Diego, CA) was used in this study, similar to a study by El Ali et al. [17]. First, an MDA conjugate was coated on an ELISA plate. The unknown MDA protein samples or MDA-BSA standards were then added to the MDA conjugate on a preabsorbed ELISA plate. After a brief incubation, an anti-MDA polyclonal antibody was added, followed by an HRP conjugated secondary antibody. The absorbance was measured at 450 nm. The content of MDA protein adducts in unknown samples was determined by comparison with a

predetermined MDA–BSA standard curve. Values were expressed in terms of MDA pmol/mg protein.

### 2.10. Protein oxidation

A 3-NT ELISA kit (Abcam, Cambridge, MA) was used for detection and quantification of 3-NT in cell lysates. The assay employs an antibody specific for 3-NT coated on a 96-well plate. Standards and samples were pipetted into the wells and 3-NT present in the sample was bound to the wells by the immobilized antibody. The wells were washed and a biotin-labeled anti-3-NT detector antibody was added. After washing away unbound detector antibody, HPR-conjugated streptavidin specific for biotin labeled detector antibody was pipetted into the wells. The blue color developed after addition of a TMB (3,3′,5,5′-tetramethylbenzidine) substrate to the washed wells was measured at 600 nm. The protein 3-NT content in unknown samples was determined by comparing with a standard curve that was prepared from predetermined 3-NT BSA standards.

### 2.11. Gold labeling immunoelectron microscopy

Brain tissue was removed and cut to size of about 2 cm and 3–5 mm thick then fixed in 4% paraformaldehyde + 0.1% glutaraldehyde in 0.1 M phosphate buffer (PB) for 1 h at room temperature or at 4 °C, and then washed thoroughly with PB (pH 7.3). Tissue was trimmed further to 1–2 mm pieces. Osmication was omitted for labeling procedures. Dehydration was in an ethanol series (50%, 70%, 80%, at 15 min each). Tissue was placed in 2:1 LR White resin (Electron Microscopy Sciences, PA) to 70% ethanol for 1 h to avoid tissue shrinkage, and then further infiltrated in 100% LR White for 1 h, overnight, and then two changes for 30 min. Tissue was added to gelatin capsules and LR White polymerized at 50 °C for 24 h. Gold–silver sections were placed on nickel grids coated with Formvar or colloidin. Sections on grids were protein-blocked in Aurion goat gold conjugate (Electron Microscopy Sciences, PA) for 30 min and washed in PBS–0.2% bovine serum albumin 3× for 5 min at pH 7.4 (Electron Microscopy Sciences, PA). Aurion ultra small gold conjugate–goat antibiotin (Electron Microscopy Sciences, PA) in PBS–0.2% BSA-c was applied at 1:100 for overnight at 4 °C or for 4 h at room temperature. Grids were washed in PBS–0.2% BSA-c (pH 7.4), 6× for 5 min; in PBS, 3× for 5 min; in distilled water 5× for 2 min. Silver enhancement was done by placing grids on a droplet of Aurion R-Gent SE-EM enhancement mixture (Electron Microscopy Sciences, PA) for 90 min and then washed in distilled water. Controls involved sections with no secondary antibody (antibiotin) and no silver enhancement. Sections were stained with uranyl acetate for 15 min followed by lead citrate for 3 min. Sections were viewed with a Zeiss T109 electron microscope with Gatan digital micrograph software operated at 80 kV.

### 2.12. High performance liquid chromatography (HPLC) analysis of OKN-007 in rat brain tissues

OKN-007 was extracted from normal (contralateral brain tissue) and glioma tumor tissue lysates in methanol to precipitate tissue proteins following centrifugation at 14,000 rpm for 30 min. The solvent in the supernatant was removed by centrifugal evaporation at 35–40 °C. Dried samples were reconstituted in 200 μL methanol/water (1/9 v/v) and mixed thoroughly. The extract solution was filtered through a 10,000 molecular weight cutoff filter by

centrifugation (14,000 rpm for 30 min). An aliquot was injected into an HPLC system (Hewlett-Packard 1100 HPLC system, with a C18 250 × 4.6 mm i.d. column (Supelco)) with a flow rate of 0.35 mL/min, UV detection at 297 nm, an injection volume of 5–10 μL, a mobile phase of acetonitrile/83 mM acetate buffer (pH 5.5)/water (5/75/20 v/v/v). OKN-007 eluted between 7 and 10 min. Tissue sample concentrations were determined from a standard curve.

### 2.13. Statistical analysis

Statistical differences between the probe-administered and control groups were analyzed with an unpaired, two-tailed Student *t* test using commercially available software (InStat; GraphPad Software, San Diego, CA, USA). A $P < 0.05$ was considered to indicate a statistically significant difference.

## 3. Results

Representative examples of images obtained in F98 gliomabearing rats are shown in Fig. 2. Pre- and post-DMPO probe contrast images are shown in Fig. 2A and B, respectively. A $T_2$-weighted morphological image depicts the tumor location (outlined region in Fig. 2C). A difference image illustrating increased anti-DMPO probe accumulation is shown in Fig. 2D, along with representative ROIs in the tumor and contralateral (normal) brain regions.

There were differences in the levels of macromolecular free radicals detected in the different treatment groups. OKN-007 was found to significantly decrease ($P = 0.0411$) the levels of macromolecular free radicals detected in the treated group compared to the untreated animals who were both administered the anti-DMPO probe. There was no significant difference in the level of macromolecular free radicals detected between the OKN-007-treated group and the group that received the IgG probe (negative control group) (Fig. 3A–D). Some of the anti-DMPO probe is also detected in blood vessels (depicted as small cross-sectional blood vessel regions, most notably in all three treatment groups outside the outlined tumor regions) (Figs. 3Aii–Cii). Anti-DMPO levels in the tumor regions represent uptake of the anti-DMPO probe in the tumor tissue as well as anti-DMPO probe that may be in tumor blood vessels. Some of the anti-DMPO probe is also detected in surrounding tissues, such as the muscle above the brain regions in all treatment groups (Figs. 3Aii–Cii).

The difference between the amounts of anti-DMPO probe in untreated and OKN-007-treated F98 rat gliomas was confirmed by using a streptavidin–HRP detection system (Fig. 4), whereby the streptavidin–HRP bound to the biotin moiety of the anti-DMPO probe (Fig. 1B) in excised tumor tissues. The amount of anti-DMPO probe was elevated in the UT F98 glioma rats administered with the anti-DMPO probe (Fig. 4A), but not the ones administered with OKN-007 (Fig. 5B) and/or the UT glioma-bearing rats given the nonspecific IgG contrast agent (Fig. 4C). HPLC was used to establish that OKN-007 could penetrate the blood–brain barrier in normal rat brain as well as reach rat glioma tumors (Fig. 4D.)

*Ex vivo* immunoelectron microscopy of F98 rat glioma tissues after administration of gold-labeled antibiotin was performed to determine the subcellular localization of the anti-DMPO probe (Fig. 5). The gold-labeled antibiotin was found to be distributed within the plasma

membrane, as well as the nuclei of the F98 tumor cells in rats administered the anti-DMPO *in vivo* (Fig. 5B). In comparison the control tumor cells (previously administered the nonspecific IgG contrast agent *in vivo*) only had the gold-labeled antibiotin within cell nuclei (Fig. 5A).

*Ex vivo* IHC of Nrf2 levels in untreated and OKN-007-treated F98 glioma tissue samples is shown in Fig. 6A–C. OKN-007 treatment was found to significantly ($P<0.05$) decrease the expression of Nrf2 (see Fig. 6A for representative example), compared to untreated (see Fig. 6B for representative example) F98 gliomas (Fig. 6C). *Ex vivo* IHC of inducible nitric oxide synthase (iNOS) levels in untreated and OKN-007-treated F98 glioma tissue samples is shown in Fig. 6D-E. OKN-007 treatment was found to significantly ($P<0.01$) decrease the expression of iNOS (see Fig. 6D for representative example), compared to untreated (see Fig. 6E for representative example) F98 gliomas (Fig. 6F). *Ex vivo* IHC of 3-NT (Fig. 7A–C) or MDA (Fig. 7D–F) levels in OKN-007-treated F98 gliomas also were significantly lower ($P<0.05$ for both) compared to UT rats. 3-NT levels measured via ELISA in F98 cells treated with OKN-007 were significantly lower ($P<0.05$) compared to UT F98 cells (Fig. 8A). Likewise, MDA adduct levels measured by ELISA in F98 cells treated with OKN-007 were significantly lower ($P<0.001$) compared to UT F98 cells (Fig. 8B).

## 4. Discussion

RONS are now appreciated to play a role in the signaling involved in the regulation of various physiological processes, and therefore are essential for maintaining normal cell function. However, overproduction and cumulative production of RONS can cause damage to DNA, proteins, lipids, and other macromolecules, and induce cell death. Consequently, oxidative stress and oxidative damage have been implicated in the pathogenesis and progression of many human diseases, including cancer [18]. Although the exact mechanism by which RONS promote tumorigenesis remains poorly understood, it is known that DNA damage appears to play a key role in cancer development. For instance, RONS induce DNA damage, where the reaction of free radicals with DNA generates strand breaks, base modifications, and DNA protein cross-links [2].

Apart from DNA damage, other mechanisms also have been proposed to explain the connection between free radicals and human cancer development, mutation, and transformation. One mechanism underlying these actions is the activation of transcription factors such as hypoxia inducible factor (HIF)-1α, which leads to the induction of VEGF (vascular endothelial growth factor), a key mediator of angiogenesis and tumor progression. Activation of HIF-1α also leads to the upregulation of metalloproteinases (MMP), which are important in tumor invasion and metastasis [19]. RONS also contribute to tumor survival and progression by facilitating immunosuppression. Both reactive species upregulate the activity of myeloid suppressor cells, which are abundant in the tumor microenvironment and function to inhibit antitumor adaptive immunity [20]. Furthermore, various reports have demonstrated that growth factors such as PDGF (platelet-derived growth factor) and EGF (epidermal growth factor) can stimulate RONS production. RONS, in turn, may directly or indirectly activate several mitogen-activated protein kinases (MAPKs) [21, 22], the AKT pathway [23], and the nuclear factor of kappa light polypeptide gene enhancer in B-cells

(NF-kB) [24]. Also, NF-kB induces iNOS (inducible nitric oxide synthase), leading to increased production of reactive nitrogen species, which might result in generation and accumulation of additional DNA mutations that drive tumor progression (Fig. 7) [25]. Additionally, the expression of iNOS in tumor cells induces the expressions of MMP-1 and -2, and VEGF-C and -D, and is associated with tumor growth, invasion, and lymphangiogenesis [26, 27].

All tissues and organs are susceptible to free radical damage. The human brain is especially vulnerable to free radical attack because of its high oxygen consumption and high concentrations of easily oxidizable polyunsaturated fatty acids [28]. In addition, the brain's antioxidant capacity is lower compared with other organs, and thus the brain may be more susceptible to oxidative damage [28].

Free radical scavengers, such as spin traps, have been studied by many researchers. The most widely studied spin trap agents are members of the nitrone class of free radical spin-trapping agents, in which a nitrone moiety traps ROS in addition to other radical species [29–32]. Nitrone spin traps have become increasingly attractive prospects for the treatment of a variety of pathological conditions, particularly because of the stable nitroxides that are formed after ROS trapping [30, 33]. The nitrone chemical structure in its simplest form can be represented as X–CH=NO–Y. The N–O group effectively traps oxygen, carbon, and sulfur-centered radicals to produce a stable nitroxide radical (-N–O.) [34]. The nitroxide is then readily excreted from the body via the kidneys, as is the excess nitrone [35].

OKN-007 is a nitrone free radical spin-trapping agent that has exhibited efficacy as a neuroprotectant, and is involved in the inhibition of the upregulation of inducible nitric oxide synthase and decreasing glutamate excitotoxicity [11]. OKN-007 is a small molecule that can traverse the blood–brain barrier, and has anti-inflammatory, antioxidant, and proapoptotic properties [11–36]. Our group has also established that OKN-007 is an effective anticancer agent in rodent preclinical glioma models [8–10], and it is currently undergoing clinical trial assessment as a new investigational drug for recurrent adult glioblastomas.

There are several methods that have been used to monitor the levels of free radicals *in vitro* and *in vivo*. Recently, our group reported the *in vivo* detection of free radicals in a G261 mouse glioma model by combining immunospin-trapping and molecular magnetic resonance imaging [6]. It was previously demonstrated *in vitro* that OKN-007 is an effective free radical scavenger for hydroxyl radicals [37]. In the present study we demonstrated, through the use of the combined IST and mMRI techniques, that OKN-007 was able to decrease the levels of macromolecular free radicals in a preclinical F98 rat glioma model.

Specifically, we combined mMRI with a Gd–DTPA–albumin-based contrast agent for signal detection with the specificity of an antibody for DMPO nitrone adducts (anti-DMPO probe), to detect *in vivo* macromolecular free radical levels in untreated and OKN-007-treated adult F98 rat gliomas. As a negative control, we used a nonspecific IgG antibody covalently bound to the albumin–Gd–DTPA–biotin construct. To calculate the $T_1$ relaxation, we normalized the $T_1$ relaxation values from the tumor area to the contralateral side of the brain

in each animal dataset. We used the contralateral side of the brain to normalize the $T_1$ relaxation values of the tumor region as we detected no significant difference in the $T_1$ relaxation values in the three treatment groups, 120 min after the administration of the either the anti-DMPO probe or nonspecific IgG contrast agent (UT + anti-DMPO probe, 3426 ± 322.5 ms; OKN-007 + anti-DMPO probe, 3363 ± 573.1 ms; UT + IgG probe, 3498 ± 313.0 ms). OKN-007 was found to significantly decrease ($P = 0.0411$) the levels of macromolecular free radicals in the treated group compared to the untreated animals administered with the anti-DMPO probe. There was no significant difference between the OKN-007-treated group and the group that received the IgG probe (negative control group) (Fig. 3A–D), indicating that OKN-007 reduced macromolecular free radical levels to undetectable levels. The presence of the anti-DMPO probe was also confirmed by targeting the biotin moiety of the anti-DMPO probe with streptavidin-HRP (Fig. 4A). There was little or no detection of HRP in the OKN-007-treated sample or the IgG-ad-ministered tumor tissue (Fig. 4B and C). Support regarding the effect of the ability of OKN-007 to decrease oxidative stress was also obtained from *in vitro* ELISA assessment of DCF levels in F98 cells which were either treated with OKN-007 or untreated (Fig. 8A).

We have already demonstrated with immunofluorescence that the anti-DMPO probe binds to membrane bound macromolecular free radicals in GL261 glioma tumor cells [6]. Here we also used immunoelectron microscopy to demonstrate the presence of the anti-DMPO probe in the cytoplasm/membrane and cell nuclei of F98 glioma tumor cells. In this technique, antibiotin–gold was used to bind specifically to the biotin group of the anti-DMPO probe. The IgG contrast agent, which also has a biotin moiety, was not detected with the antibiotin–gold in the plasma membrane. Likewise the level of nuclear staining was lower for the IgG contrast agent-administered sample. However, nuclei staining was found in the glioma cells administered the anti-DMPO probe. Due to the size of the anti-DMPO probe, we do not think that this probe could be taken up by the cell nuclei. There are three possible other reasons that could account for nuclear staining for biotin. It may be possible that the nuclear positive gold staining could be caused by nonspecific staining as a result of secondary labeling of biotin in newly replicated DNA [38, 39], or endogenous biotin, which has widely been taken up in the cell nuclei [40], or biotin could have come from biodegradation of the anti-DMPO probe. As the control IgG contrast agent sample had little staining for biotin, we surmise that the biotin detected in the cell nuclei from the glioma sample administered the anti-DMPO probe was from biodegradation of the probe which had accumulated in the glioma cells of untreated tumors.

OKN-007 was also found to affect some specific oxidative stress-related biomarkers. Nrf2 is an important transcriptional factor associated with cellular responses to oxidative stress [41]. Nrf2 has been found to be highly expressed in cancers and may contribute to chemoresistance [42–44]. Nrf2 may be involved as a critical transcription factor for controlling glioma angiogenesis [41]. In this study, Nrf2 levels were found to be significantly decreased ($P<0.05$) in OKN-077-treated F98 gliomas, compared to UT rats (Fig. 6A–C). Nrf2 is constitutively targeted for degradation by the $CUL3^{KEAP1}$ E3 ubiquitin ligase and the 26S proteasome. In the presence of oxidative stress, one or more cysteines of KEAP1 become oxidatively modified leading to dissociation of KEAP1 and Nrf2 from the remainder of the CUL3 ligase. Stabilized Nrf2 then translocates to the nucleus and induces

the expression of cyto-protective genes that collectively neutralize free radical stress and restore redox homeostasis. Thus, the reduced detection of Nrf2 levels following OKN-007 treatment is consistent with a reduction of free radicals by the drug, and subsequent degradation of Nrf2 by $CUL3^{KEAP1}$. Although stabilized Nrf2 is typically detected in the nucleus of cultured cells, we detected the transcription factor in both the cytoplasm and the nucleus (e.g., Fig. 6B). This may be attributed to reduced efficiency of Nrf2 nuclear translocation [45] and/or additional changes specific to disease states. Others have reported similar localization properties of the transcription factor in tumor cells [46–50]. It should also be noted that since Nfr2 levels in tumors are associated with chemoresistance [42–44, 49], OKN-077 may in addition potentially be of therapeutic benefit for chemoresistant gliomas. It has also been previously shown in ethyl nitrosourea-induced rat gliomas that IHC-detected levels of MDA and 3-NT are elevated and correlate with glioma growth [51]. In this study, in both the untreated F98 glioma tissues and the F98 cells, the levels of MDA adducts and 3-NT were found to be highly expressed, and it was determined that OKN-007 could significantly decrease both of these oxidative stress markers (see Figs. 7 and 8).

Redox pathways may be potential targets for cancer therapy. Reduced intracellular RONS levels through the administration of antioxidants impair cell proliferation and survival in some types of cancers, such as gliomas [52], colorectal cancer [53], and lymphomas [54]. Martín et al. demonstrated that *N*-acetylcysteine could decrease C6 glioma cell proliferation, inducing a cell cycle arrest in the $G_0/G_1$ phase and markedly upregulating p21 expression [52]. *N*-Acetylcysteine also decreased AKT activity, extracellular signal-regulated kinase 1/2, and the redoxsensitive transcription factor NF-κB, all of which are RONS related, and seem to be in close connection with cell proliferation [52].

OKN-007 may share some of the antioxidant mechanisms of action of *N*-acetylcysteine. It has been previously shown that nitrones decrease iNOS activity (Fig. 9) [55], which occur in brain tumors [56]. We also found that OKN-007 decreases iNOS in F98 glioma-bearing rat tissues with IHC (Figs. D–F). Furthermore, they can also downregulate cytokines [tumor necrosis factor alpha (TNF-α), interferon-gamma (IFN-γ)], and NF-κB expression [57], which promotes iNOS expression (Fig. 7) [58]. Our data also suggest that the inhibition of the tumor growth by OKN-007 in different preclinical glioma models, as we have reported previously [8–10], may in part be due to the reduction of free radicals, as demonstrated in this study on F98 gliomas. IHC assessment of commonly studied tumor markers for cell proliferation or differentiation, hypoxia, angiogenesis, and apoptosis indicated that OKN-007 was able to significantly decrease cell proliferation (glucose transporter 1 (Glut-1) and the cell proliferation marker, MIB-1) but not cell differentiation (carbonate anhydrase IX), decrease angiogenesis (microvessel density (MVD; measured as levels of the endothelial marker, CD-31), but not the VEGF), decrease HIF-1α, and increase apoptosis (cleaved caspase 3) compared with untreated controls [8]. OKN-007-induced decreases in Glut-1 and HIF-1α levels seemed to be similar in both F98 and U87 glioma models, whereas increased apoptosis seemed to be more elevated in the F98 gliomas compared to the U87 tumors [8]. From these studies we concluded that OKN-007 has the ability to cause glioma regression in aggressive rodent tumor models (F98 and U87), as well as in moderate gliomas (C6) [8–10]. Support for the anticancer effect of OKN-007 via the transforming growth factor β1 (TGFβ1) pathway was reported by Zheng et al., where they found that OKN-007

mediates its antitumor effect in hepatocellular carcinoma cells (Huh7) via the suppression of TGFβ1/SMAD2 and Hedgehog/GLI1 signaling by inhibiting sulfatase 2 (SULF2) enzymatic activity [59].

## 5. Conclusions

This is the first attempt at detecting *in vivo* levels of macromolecular radicals from a rat glioma model and assessing the free radical scavenging capability of a nitrone anticancer agent. OKN-007 was found to dramatically reduce macromolecular free radical levels compared to untreated gliomas. mMRl provides the advantage of *in vivo* image resolution as well as the assessment of the spatial location of oxidative stress events in heterogeneous tissues or organs.

This method can potentially be applied toward other types of cancers for the *in vivo* assessment of macromolecular free radical levels. The results indicate that OKN-007 treatment substantially decreased free radical levels in a F98 rat glioma model.

## Acknowledgments

We gratefully acknowledge Mr. Hirst Holloway for his help during all stages of the project. We also thank the Peggy and Charles Stephenson Cancer Center at the University of Oklahoma, Oklahoma City, OK, for use of their Histology and Immunohistochemistry Core for cryosectioning, funded by an Institutional Development Award (IDeA) from the National Institute of General Medical Sciences of the National Institutes of Health under grant number P20 GM103639. This work was also supported by the Oklahoma Medical Research Foundation (R.A.T.) and the National Institute of Environmental Health Sciences (R.P.M.).

## Abbreviations

| | |
|---|---|
| **BSA** | bovine serum albumin |
| **CNS** | central nervous system |
| **ERK 1/2** | extracellular signal-regulated kinase 1/2 |
| **DMPO** | 5,5-dimethyl-1-pyrroline N-oxide |
| **DTPA** | diethylene triamine penta acetic acid |
| **EGF** | epidermal growth factor |
| **Gd** | gadolinium |
| **HIF-1α** | hypoxia inducible factor-1α |
| **IFN-γ** | interferon-gamma |
| **IHC** | immunohistochemistry |
| **iNOS** | inducible nitric oxide synthase |
| **IST** | immuno-spin trapping |
| **MDA** | malondialdehyde |

| | |
|---|---|
| **MMP** | metalloproteinase |
| **MRI** | magnetic resonance imaging |
| **mMRI** | molecular magnetic resonance imaging |
| **NO** | nitric oxide |
| **NF-kB** | nuclear factor of kappa light polypeptide gene enhancer in B-cells |
| **Nrf2** | nuclear factor erythroid 2-related factor 2 |
| **3-NT** | 3-nitrotyrosine |
| **OKN-007** | Oklahoma nitrone-007 (2, 4-disulfophenyl-PBN or disodium 4-[(tert-butyl-imino) methyl] |
| **benzene-1** | 3-disulfonate N-oxide or disufenton also previously known as NXY-059) |
| **ONOO–** | peroxynitrite |
| **O2-** | superoxide anion |
| **PDGF** | platelet-derived growth factor |
| **RARE** | Rapid acquisition with relaxation enhancement |
| **RONS** | reactive oxygen and nitrogen species |
| **RNS** | reactive nitrogen species |
| **ROI** | region of interest |
| **ROS** | reactive oxygen species |
| **TE** | echo time |
| **TNF-α** | tumor necrosis factor alpha |
| **TR** | repetition time |
| **VEGF** | vascular endothelial growth factor |
| **UT** | untreated |

## References

[1]. Pala FS, Gürkan H, The role of free radicals in ethiopathogenesis of diseases, Adv. Mol. Biol 1 (2008) 1–9.

[2]. Lobo V, Patil A, Phatak A, Chandra N, Free radicals, antioxidants and functional foods: Impact on human health, Pharmacogn. Rev 4 (8) (2010) 118–126. [PubMed: 22228951]

[3]. Devi GS, Prasad MH, Saraswathi I, Raghu D, Rao DN, Reddy PP, Free radicals antioxidant enzymes and lipid peroxidation in different types of leukemias, Clin. Chim. Acta 293 (1–2) (2000) 53–62. [PubMed: 10699422]

[4]. McCord JM, The evolution of free radicals and oxidative stress, Am. J. Med 108 (8) (2000) 652–659. [PubMed: 10856414]

[5]. Pham-Huy LA, He H, Pham-Huy C, Free radicals, antioxidants in disease and health, Int. J. Biomed. Sci 4 (2) (2008) 89–96. [PubMed: 23675073]

[6]. Towner RA, Smith N, Saunders D, De Souza PC, Henry L, Lupu F, Silasi-Mansat R, Ehrenshaft M, Mason RP, Gomez-Mejiba SE, Ramirez DC, Combined molecular MRI and immunospin-trapping for in vivo detection of free radicals in orthotopic mouse GL261 gliomas, Biochim. Biophys. Acta 1832 (12) (2013) 2153–2161. [PubMed: 23959048]

[7]. Towner RA, Smith N, Saunders D, Henderson M, Downum K, Lupu F, Silasi-Mansat R, Ramirez DC, Gomez-Mejiba SE, Bonini MG, Ehrenshaft M, Mason RP, In vivo imaging of immunospin trapped radicals with molecular magnetic resonance imaging in a diabetic mouse model, Diabetes 61 (10) (2012) 2405–2413. [PubMed: 22698922]

[8]. Towner RA, Gillespie DL, Schwager A, Saunders DG, Smith N, Njoku CE, Krysiak RS, 3rd, Larabee C, Iqbal H, Floyd RA, Bourne DW, Abdullah O, Hsu EW, Jensen RL, Regression of glioma tumor growth in F98 and U87 rat glioma models by the Nitrone OKN-007, Neuro Oncol 15 (3) (2013) 330–340. [PubMed: 23328810]

[9]. He T, Doblas S, Saunders D, Casteel R, Lerner M, Ritchey JW, Snider T, Floyd RA, Towner RA, Effects of PBN and OKN007 in rodent glioma models assessed by 1H MR spectroscopy, Free Radic. Biol. Med 51 (2) (2011) 490–502. [PubMed: 21600283]

[10]. Garteiser P, Doblas S, Watanabe Y, Saunders D, Hoyle J, Lerner M, He T, Floyd RA, Towner RA, Multiparametric assessment of the anti-glioma properties of OKN007 by magnetic resonance imaging, J. Magn. Reson. Imaging 31 (4) (2010) 796–806. [PubMed: 20373422]

[11]. Floyd RA, Kopke RD, Choi CH, Foster SB, Doblas S, Towner RA, Nitrones as therapeutics, Free Radic. Biol. Med 45 (10) (2008) 1361–1374. [PubMed: 18793715]

[12]. Dafni H, Landsman L, Schechter B, Kohen F, Neeman M, MRI and fluorescence microscopy of the acute vascular response to VEGF165: vasodilation, hyper-permeability and lymphatic uptake, followed by rapid inactivation of the growth factor, NMR Biomed 15 (2) (2002) 120–131. [PubMed: 11870908]

[13]. Towner RA, Smith N, Doblas S, Tesiram Y, Garteiser P, Saunders D, Cranford R, Silasi-Mansat R, Herlea O, Ivanciu L, Wu D, Lupu F, In vivo detection of c-Met expression in a rat C6 glioma model, J. Cell. Mol. Med 12 (1) (2008) 174–186. [PubMed: 18194445]

[14]. Hermanson GT, Bioconjugate techniques, Academic Press, San Diego, 1996.

[15]. Haacke EM, Magnetic resonance imaging: physical principles and sequence design , Wiley-Liss, New York, 1999.

[16]. Forman HJ, Augusto O, Brigelius-Flohe R, Dennery PA, Kalyanaraman B, Ischiropoulos H, Mann GE, Radi R, Roberts LJ, II, Vina J, Davies KJA. Even free radicals should follow some rules: a guide to free radical research terminology and methodology, Free Radic. Biol. Med 78(2015) 233–235. [PubMed: 25462642]

[17]. El Ali A, Doeppner TR, Zechariah A, Hermann DM. Increased blood-brain barrier permeability and brain edema after focal cerebral ischemia induced by hyperlipidemia: role of lipid peroxidation and calpain-1/2, matrix metalloproteinase-2/9, and RhoA overactivation, Stroke 42(2011) 3238–3244. [PubMed: 21836084]

[18]. Holmstrom KM, Finkel T, Cellular mechanisms and physiological consequences of redox-dependent signalling, Nat. Rev. Mol. Cell. Biol 15 (6) (2014) 411–421. [PubMed: 24854789]

[19]. Halliwell B, Biochemistry of oxidative stress, Biochem. Soc. Trans 35 (Pt 5) (2007) 1147–1150. [PubMed: 17956298]

[20]. Mantovani A, Sica A, Allavena P, Garlanda C, Locati M, Tumor-associated macrophages and the related myeloid-derived suppressor cells as a paradigm of the diversity of macrophage activation, Hum. Immunol 70 (5) (2009) 325–330. [PubMed: 19236898]

[21]. Mesquita FS, Dyer SN, Heinrich DA, Bulun SE, Marsh EE, Nowak RA, Reactive oxygen species mediate mitogenic growth factor signaling pathways in human leiomyoma smooth muscle cells, Biol. Reprod 82 (2) (2010) 341–351. [PubMed: 19741209]

[22]. Sundaresan M, Yu ZX, Ferrans VJ, Irani K, Finkel T, Requirement for generation of $H_2O_2$ for platelet-derived growth factor signal transduction, Science 270 (5234) (1995) 296–269. [PubMed: 7569979]

[23]. Mochizuki T, Furuta S, Mitsushita J, Shang WH, Ito M, Yokoo Y, Yamaura M, Ishizone S, Nakayama J, Konagai A, Hirose K, Kiyosawa K, Kamata T, Inhibition of NADPH oxidase 4 activates apoptosis via the AKT/apoptosis signal-regulating kinase 1 pathway in pancreatic cancer PANC-1 cells, Oncogene 25 (26) (2006) 3699–3707. [PubMed: 16532036]

[24]. Deshpande SS, Angkeow P, Huang J, Ozaki M, Irani KRac1 inhibits TNF-alpha-induced endothelial cell apoptosis: dual regulation by reactive oxygen species. FASEB J 200; 14 (12): 1705–1714.

[25]. Bogdan C, Nitric oxide and the immune response, Nat. Immunol 2 (10) (2001) 907–916. [PubMed: 11577346]

[26]. Nakamura Y, Yasuoka H, Tsujimoto M, Yoshidome K, Nakahara M, Nakao K, Nakamura M, Kakudo K, Nitric oxide in breast cancer: induction of vascular endothelial growth factor-C and correlation with metastasis and poor prognosis, Clin. Cancer Res 12 (4) (2006) 1201–1207. [PubMed: 16489074]

[27]. Viswanathan AN, Feskanich D, Schernhammer ES, Hankinson SE, Aspirin, NSAID, and acetaminophen use and the risk of endometrial cancer, Cancer Res 68 (7) (2008) 2507–2513. [PubMed: 18381460]

[28]. Halliwell B, Gutteridge JM Free radicals in biology and medicine. Oxford: Oxford UP; 2007.

[29]. Anderson KM, Ells G, Bonomi P, Harris JE, Free radical spin traps as adjuncts for the prevention and treatment of disease, Med. Hypotheses 52 (1) (1999) 53–57. [PubMed: 10342672]

[30]. Becker DA, Diagnostic and therapeutic applications of azulenyl nitrone spin traps, Cell Mol. Life Sci 56 (7–8) (1999) 626–633. [PubMed: 11212310]

[31]. Floyd RA, Antioxidants, oxidative stress, and degenerative neurological disorders, Proc. Soc. Exp. Biol. Med 222 (3) (1999) 236–245. [PubMed: 10601882]

[32]. Hensley K, Carney JM, Stewart CA, Tabatabaie T, Pye Q, Floyd RA, Nitrone-based free radical traps as neuroprotective agents in cerebral ischaemia and other pathologies, Int. Rev. Neurobiol 40(1997) 299–317. [PubMed: 8989626]

[33]. Lapchak PA, Araujo DM, Reducing bleeding complications after thrombolytic therapy for stroke: clinical potential of metalloproteinase inhibitors and spin trap agents, CNS Drugs 15 (1) (2001) 819–829. [PubMed: 11700147]

[34]. Lapchak PA, Araujo DM, Song D, Wei J, Zivin JA, Neuroprotective effects of the spin trap agent disodium-[(*tert*–butylimino)methyl]benzene-1,3-disulfonate N-oxide (generic NXY-059) in a rabbit small clot embolic stroke model: Combination studies with the thrombolytic tissue plasminogen activator, Stroke 33 (5) (2002) 1411–1415. [PubMed: 11988623]

[35]. Lapchak PA, Araujo DM, Development of the nitrone-based spin trap agent NXY-059 to treat acute ischemic stroke, CNS Drug Rev 9 (3) (2003) 253–262. [PubMed: 14530797]

[36]. Floyd RA, Chandru HK, He T, Towner R, Anti-cancer activity of nitrones and observations on mechanism of action, Anti cancer Agents Med. Chem 11 (4) (2011) 373–379.

[37]. Williams HE, Claybourn M, Green AR, Investigating the free radical trapping ability of NXY-059, S-PBN and PBN, Free Radic. Res 41 (9) (2007) 1047–1052. [PubMed: 17729123]

[38]. Zempleni J, Uptake, localization, and noncarboxylase roles of biotin, Annu. Rev. Nutr 25(2005) 175–196. [PubMed: 16011464]

[39]. Hiriyanna KT, Varkey J, Beer M, Benbow RM, Electron microscopic visualization of sites of nascent DNA synthesis by streptavidin-gold binding to biotinylated nucleotides incorporated in vivo, J. Cell Biol 107 (1) (1988) 33–44. [PubMed: 3392102]

[40]. Nikiel B, Chekan M, Jarzab M, Lange D, Endogenous avidin biotin activity (EABA) in thyroid pathology: immunohistochemical study, Thyroid Res 2 (1) (2009) 5. [PubMed: 19351422]

[41]. Ji X, Wang H, Zhu J, Zhu L, Pan H, Li W, Zhou Y, Cong Z, Yan F, Chen S, Knockdown of Nrf2 suppresses glioblastoma angiogenesis by inhibiting hypoxia-induced activation of HIF-1α, Int. J. Cancer 135 (2014) 574–584. [PubMed: 24374745]

[42]. Lau A, Villeneuve NF, Sun Z, Wong PK, Zhang DD, Dual roles of Nrf2 in cancer, Pharmacol. Res 58 (5-6) (2008) 262–270. [PubMed: 18838122]

[43]. Hayes JD, McMahon M, The double-edged sword of Nrf2: subversion of redox homeostasis during the evolution of cancer, Mol. Cell 21(2006) 732–734. [PubMed: 16543142]

[44]. Kensler TW, Wakabayashi N, Nrf2: friend or foe for chemoprevention? Carcinogenesis 31(2010) 90–99. [PubMed: 19793802]

[45]. Bitar MS, Liu C, Ziaei A, Chen Y, Schmedt T, Jurkunas UV, Decline in DJ-1 and decreased nuclear translocation of Nrf2 in Fuchs endothelial corneal dystrophy, Investigative Ophthalmol. Vis. Sci 53(2012) 5806–5813.

[46]. Ji L, Wei Y, Jiang T, Wang S, Correlation of Nrf2, NQO1, MRP1, cmycs and p53 in colorectal cancer and their relationship to clinicopathologic features and survival, Int. J. Clin. Exp. Pathol 7(2014) 1124–1131. [PubMed: 24695690]

[47]. Santacana M, Maiques O, Valls J, Gatius S, Abó AI, López-Garcia MÁ, Mota A, Reventós J, Moreno-Bueno G, Palacios J, Bartosch C, Dolcet X, Matias-Guiu X, A 9-protein biomarker molecular signature for predicting histologic type in endometrial carcinoma by immunohistochemistry, Hum. Pathol 45(2014) 2394–2403. [PubMed: 25282036]

[48]. Huang CF, Zhang L, Ma SR, Zhao ZL, Wang WM, He KF, Zhao YF, Zhang WF, Liu B, Sun ZJ, Clinical significance of Keap1 and Nrf2 in oral squamous cell carcinoma, PLoS One 8 (12) (2013) e83479. [PubMed: 24386210]

[49]. Hu XF, Yao J, Gao SG, Wang XS, Peng XQ, Yang YT, Feng XS, Nrf2 overexpression predicts prognosis and f-FU resistance in gastric cancer, Asian Pac J. Cancer Prev 14(2013) 5231–5235. [PubMed: 24175806]

[50]. Park JY, Kim YW, Park YK, Nrf2 expression is associated with poor outcome in osteosarcoma, Pathology 44(2012) 617–621. [PubMed: 23172081]

[51]. Mahlke MA, Cortez LA, Ortiz MA, Rodriguez M, Uchida K, Shigenaga MK, Lee S, Zhang Y, Tominaga K, Hubbard GB, Ikeno Y, The anti-tumor effects of calorie restriction are correlated with reduced oxidative stress in ENU-induced gliomas, Pathobiol. Aging Age Relat. Dis 1(2011) 7189.

[52]. Martin V, Herrera F, Garcia-Santos G, Antolin I, Rodriguez-Blanco J, Rodriguez C, Signaling pathways involved in antioxidant control of glioma cell proliferation, Free Radic. Biol. Med 42 (11) (2007) 1715–1722. [PubMed: 17462539]

[53]. Chinery R, Beauchamp RD, Shyr Y, Kirkland SC, Coffey RJ, Morrow JD, Antioxidants reduce cyclooxygenase-2 expression, prostaglandin production, and proliferation in colorectal cancer cells, Cancer Res 58 (11) (1998) 2323–2327. [PubMed: 9622066]

[54]. Sharma R, Vinayak M, Antioxidant alpha-tocopherol checks lymphoma promotion via regulation of expression of protein kinase C-alpha and c-Myc genes and glycolytic metabolism, Leuk. Lymphoma 53 (6) (2012) 1203–1210. [PubMed: 22132835]

[55]. Tabatabaie T, Graham KL, Vasquez AM, Floyd RA, Kotake Y, Inhibition of the cytokine-mediated inducible nitric oxide synthase expression in rat insulinoma cells by phenyl N-*tert*-butylnitrone, Nitric Oxide 4 (2) (2000) 157–167. [PubMed: 10835296]

[56]. Cobbs CS, Brenman JE, Aldape KD, Bredt DS, Israel MA, Expression of nitric oxide synthase in human central nervous system tumors, Cancer Res 55 (4) (1995) 727–730. [PubMed: 7531613]

[57]. Pogrebniak HW, Merino MJ, Hahn SM, Mitchell JB, Pass HI, Spin trap salvage from endotoxemia: the role of cytokine down-regulation, Surgery 112 (2) (1992) 130–139. [PubMed: 1641756]

[58]. Xie QW, Whisnant R, Nathan C, Promoter of the mouse gene encoding calciumin-dependent nitric oxide synthase confers inducibility by interferon gamma and bacterial lipopolysaccharide, J. Exp. Med 177 (6) (1993) 1779–1784. [PubMed: 7684434]

[59]. Zheng X, Gai X, Han S, Moser CD, Hu C, Shire AM, Floyd RA, Roberts LR, The human sulfatase 2 inhibitor 2,4-disulfonylphenyl-*tert*-butylnitrone(OKN-007) has an antitumor effect in hepatocellular carcinoma mediated via suppression of TGFB1/SMAD2 and Hedgehog/GLI1 signaling, Genes Chromosomes Cancer 52(2013) 225–236. [PubMed: 23109092]

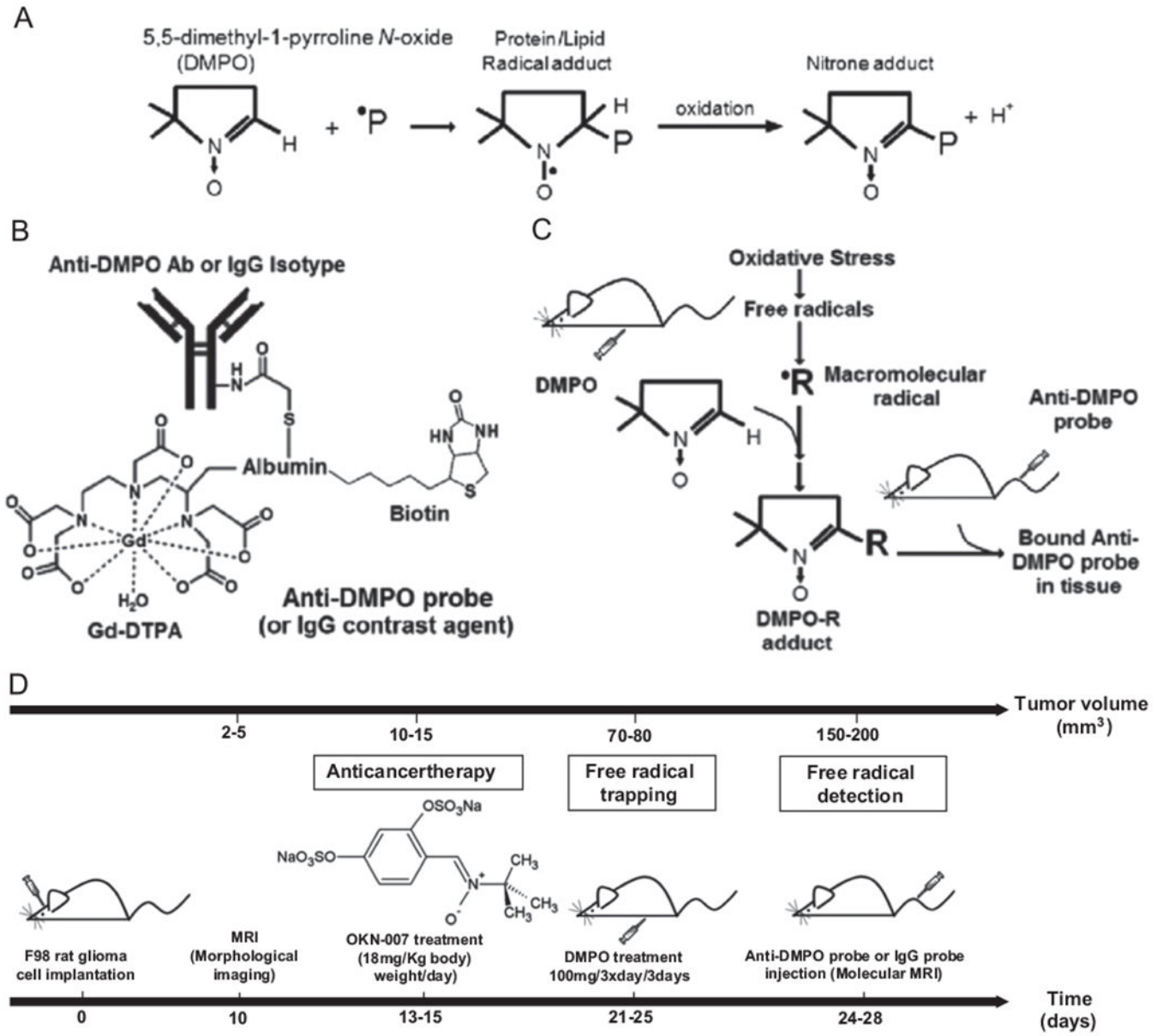


**Fig. 1.**

Approach for combined in vivo mMRI and IST. (A) Free radicals that are generated as a result of oxidative stress processes can be trapped by the spin-trapping compound, 5,5-dimethyl-1-pyrroline *N*-oxide (DMPO), to form DMPO-R adducts, which can be further assessed by immunospin trapping (IST), a method that uses an antibody against DMPO-nitrone adducts. (B) Schematic structure of anti-DMPO probe or nonspecific IgG contrast agent. (C) Immunospin trapping of free radicals (●R) with mMRI anti-DMPO probe. DMPO is injected ip to trap free radicals and generate nitrone-radical (R) adducts. Anti-DMPO is injected iv to target nitrone-R adducts, which can be visualized by mMRI. Modified from Biochimica et Biophysica Acta, 1832(12), Towner RA et al. (2013) [6]. Copyright (2013), with permission from Elsevier. (D) Schematic representation of the timeline for the experimental procedures used in this study. Top timeline represents tumor

volumes ($mm^3$), and the bottom timeline refers to the procedures performed (days). F98 rat glioma cell implantation was performed on day 0. Morphological ($T_2$-weighted) MRI scans were started 10 days after the F98 cell implantation and were performed every 2–3 days until the end of the study. OKN-007 treatment (anticancer therapy) was initiated when the tumor volumes were between 10 and 15 $mm^3$. DMPO administration (100 mg diluted in 200 μL of saline) (free radical trapping) was started when the tumor volumes were between 70 and 80 $mm^3$. After DMPO treatment (at 24–28 days post F98 cell implantation), injection of the anti-DMPO probe was done to detect the presence of free radicals, or the IgG contrast agent was administered as a control.

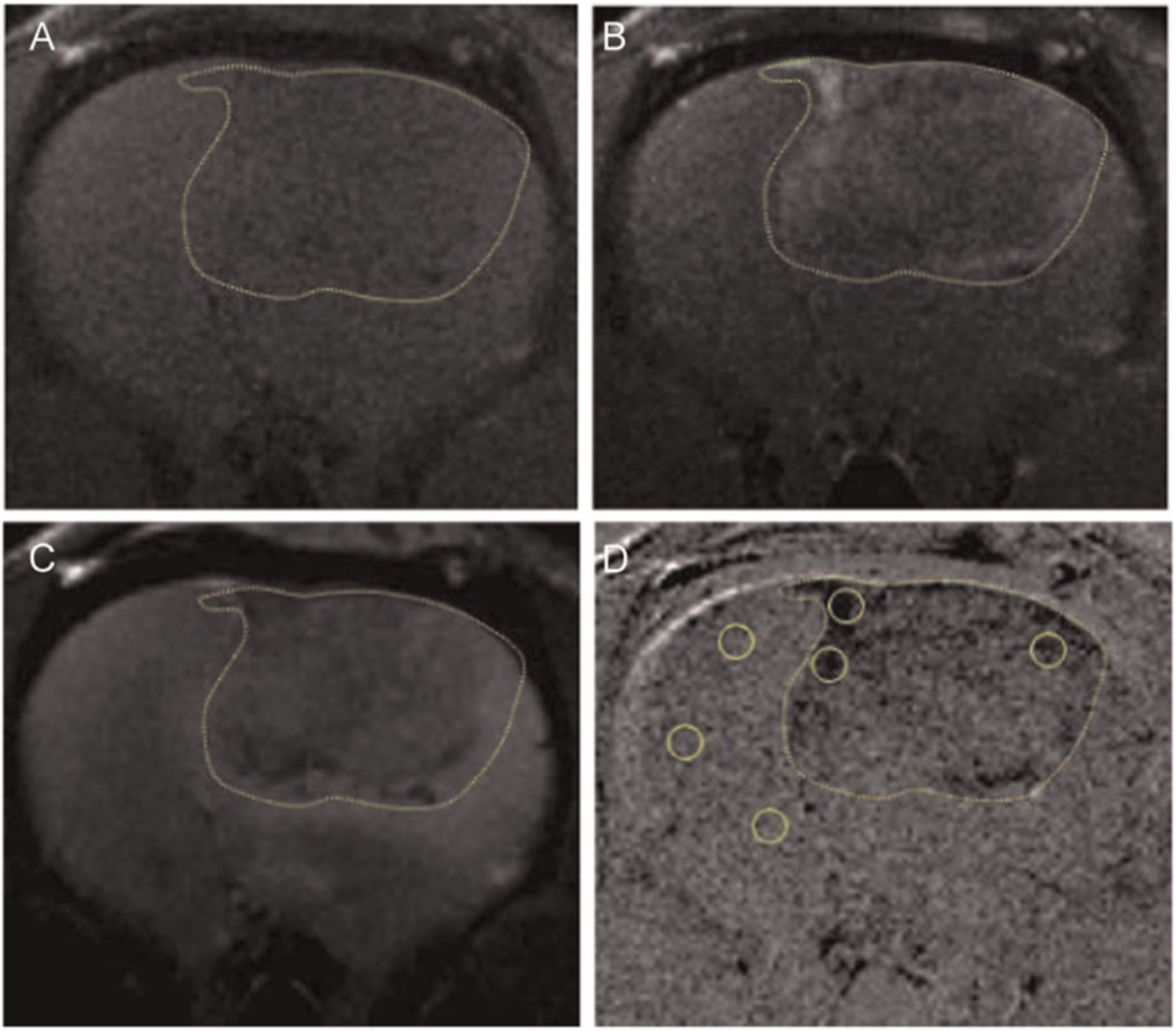


**Fig. 2.**

Morphological MR images obtained before and 2 h after injection of anti-DMPO probe (contrast agent) in a F98 rat glioma moldel. (A) Representative $T_1$-weighted image before injection of the anti-DMPO probe. (B) Representative $T_1$-weighted image 2 h after injection of the anti-DMPO probe. (C) Representative $T_2$-weighted image of F98 rat glioma. (D) Representative difference image, which is the subtraction between the $T_1$ images of pre- and 2 h after injection of the contrast agent (A,B). The dark regions in the tumor depict areas of increased uptake of the anti-DMPO probe. Representative ROIs in the tumor and contralateral side of the brain are illustrated as circles in each region. The tumor is delineated by a dashed line in each panel.

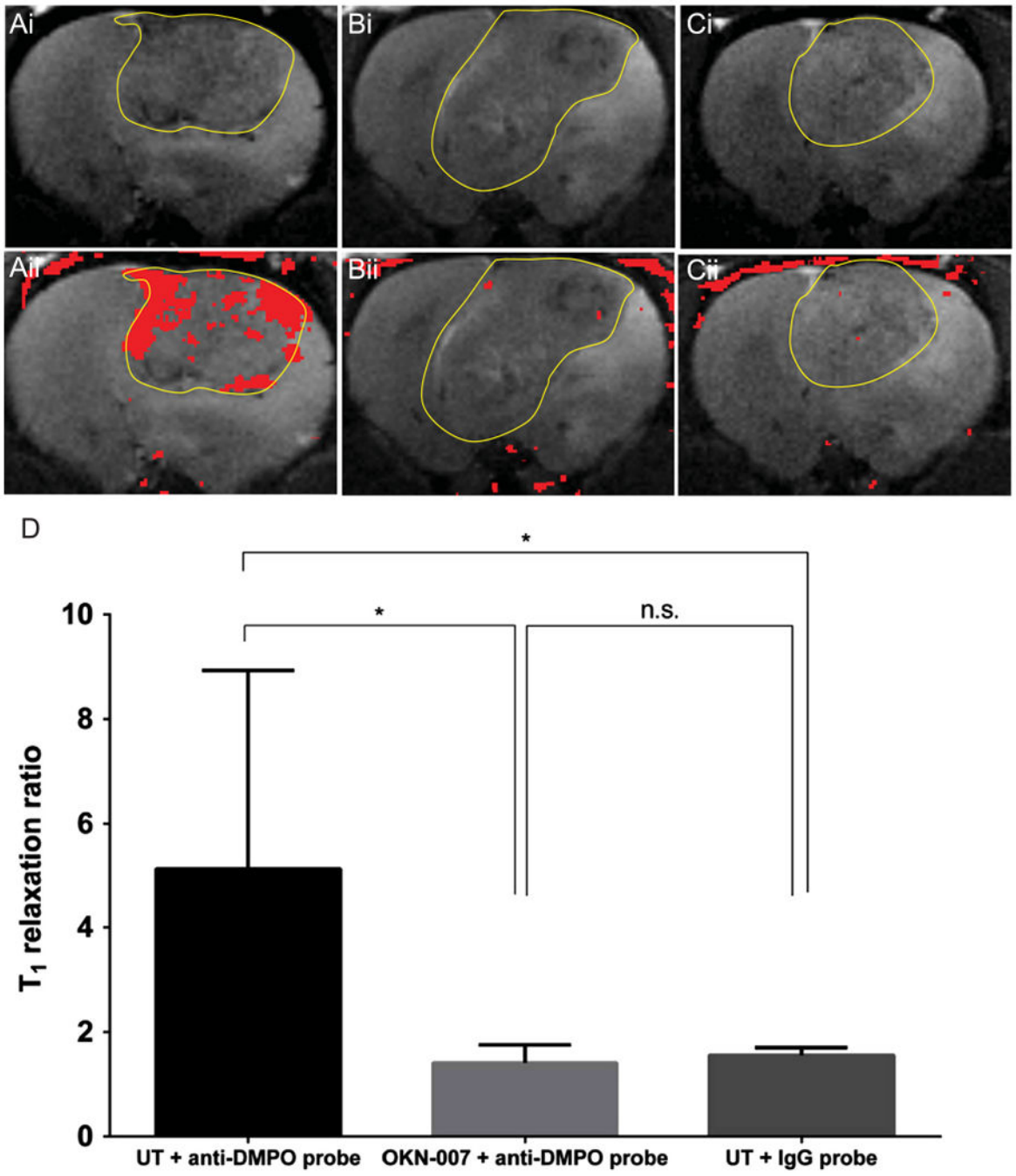


**Fig. 3.**

mMRI detection of free radical adducts in a F98 rat glioma model. Representative MR images from: (A) untreated + anti-DMPO probe, (B) OKN treatment + anti-DMPO probe, (C) untreated + IgG probe, treated F98 rat gliomas. (A-Ci) $T_2$-weighted images of F98 glioma. (A–Cii) $T_2$-weighted images overlayed with a difference $T_1$-weighted image (red), which was the subtraction between the 2 h postcontrast and the precontrast images after injection of either the anti-DMPO probe or the IgG contrast agent. Overlays of the contrast difference images and the $T_2$-weighed images were generated using the 3D Analysis

Software for Life Sciences Amira. Red regions indicate the presence of the anti-DMPO probe or the IgG contrast agent. Outside the outlined tumor regions the detection of the anti-DMPO probe can occur in blood vessels (small regions depicting blood vessel cross sections) and surrounding muscle tissues (top regions). (D) OKN-007 was found to significantly decrease ($P = 0.0411$) (1.407 ± 0.1548, $n=5$) the levels of free radicals in the treated group compared to the untreated animals (5.131 ± 1.437, $n=7$), which both received the anti-DMPO probe. There was no significant difference between the OKN-007-treated group and the untreated animals that received the IgG contrast (negative control group). Values are represented as means ± SD. Asterisks indicate statistically significant differences (*$P < 0.05$). UT: untreated animals.

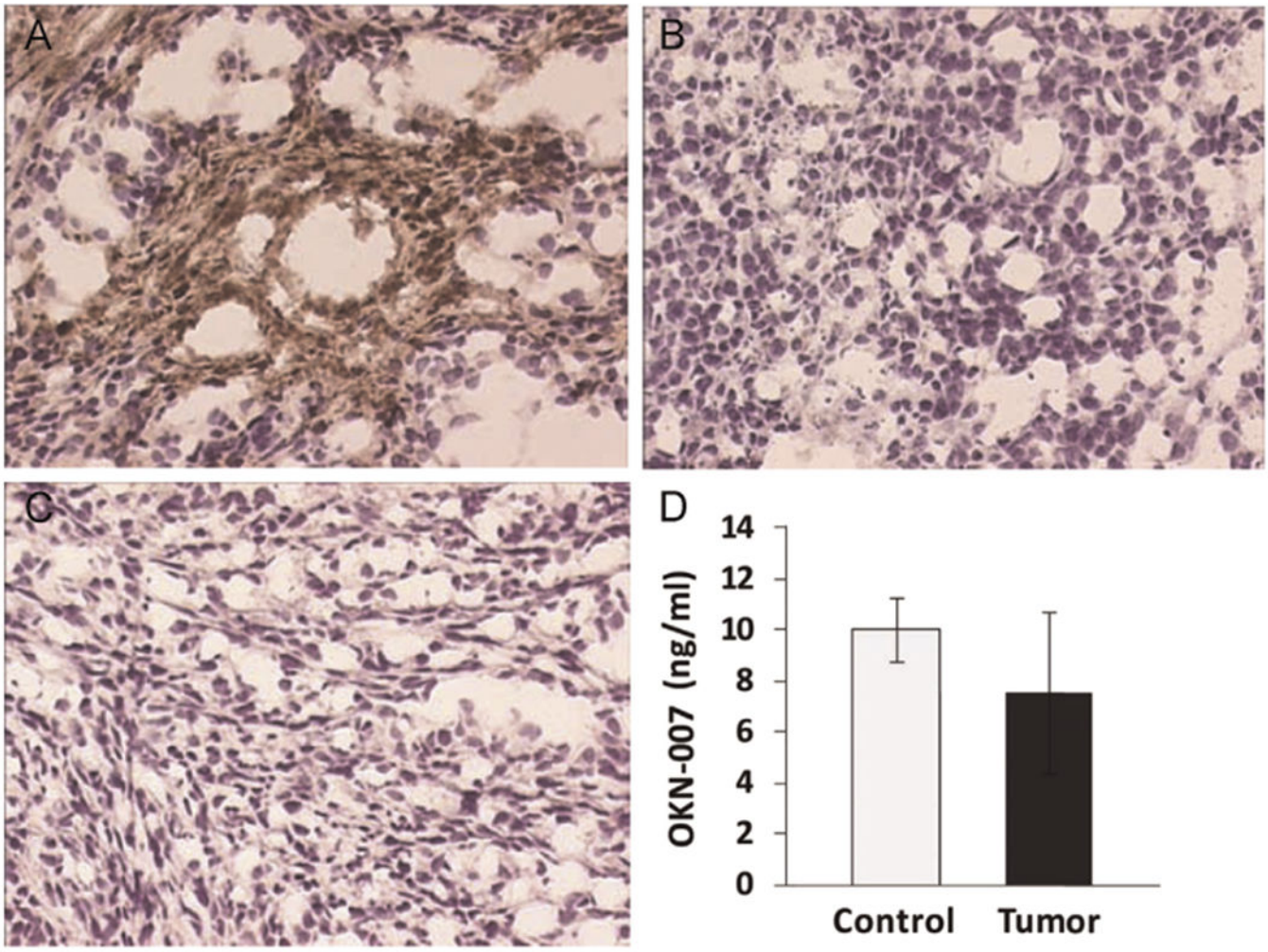


**Fig. 4.**

*Ex vivo* detection of the anti-DMPO probe in F98 rat gliomas with streptavidin horseradish peroxidase (HRP), and detection of OKN-007 in brain tissues. Streptavidin–HRP binds to the biotin moiety of the anti-DMPO probe. The detection of the anti-DMPO probe is elevated in untreated F98 gliomas administered with the anti-DMPO probe (A, brown stain), but not for those treated with OKN-007 (B). There is no detection of sustained nonspecific IgG contrast agent with streptavidin–HRP (C). Magnification = 200×. (D) High performance liquid chromatography (HPLC)-derived brain tissue levels (concentration in ng/ml of tissue lysate) of OKN-007 following oral administration (via gavage; 18 mg/kg (0.015% w/v)) in glioma tumor (Tumor) and contralateral normal brain (Control) tissues in rat glioma-bearing rats. OKN-007 was found to be equally taken up in normal brain and tumor tissues.

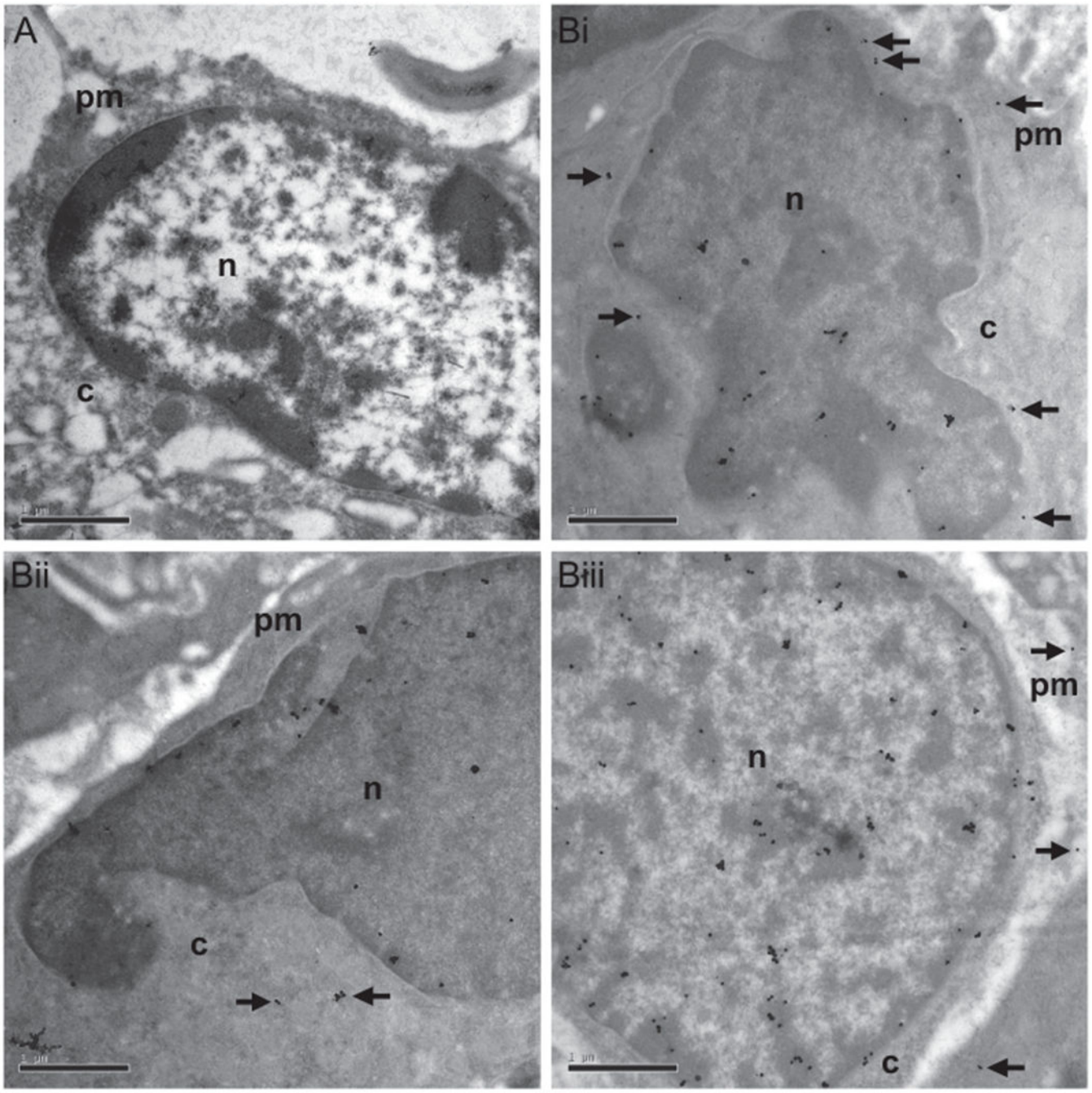


**Fig. 5.**

Immunoelectron microscopy detection of the anti-DMPO probe in the plasma membrane/cytoplasm and cell nuclei in F98 rat gliomas. The biotin moiety of the anti-DMPO probe was targeted with gold–antibiotin. (A) F98 glioma tumor cells administered a nonspecific IgG contrast agent *in vivo*, and stained with gold–antibiotin. Note no detection of gold–antibiotin colloid in either the plasma membrane/cytoplasm or the cell nucleus. (Bi–iii) Gold–antibiotin colloids were detected within the plasma membrane/cytoplasm (black

arrows) and cell nuclei of F98 tumor cells administered the anti-DMPO probe. Scale bar = 1 μm. Magnification = 20,000×. *n* = nucleus; *c* = cytoplasm; pm = plasma membrane.

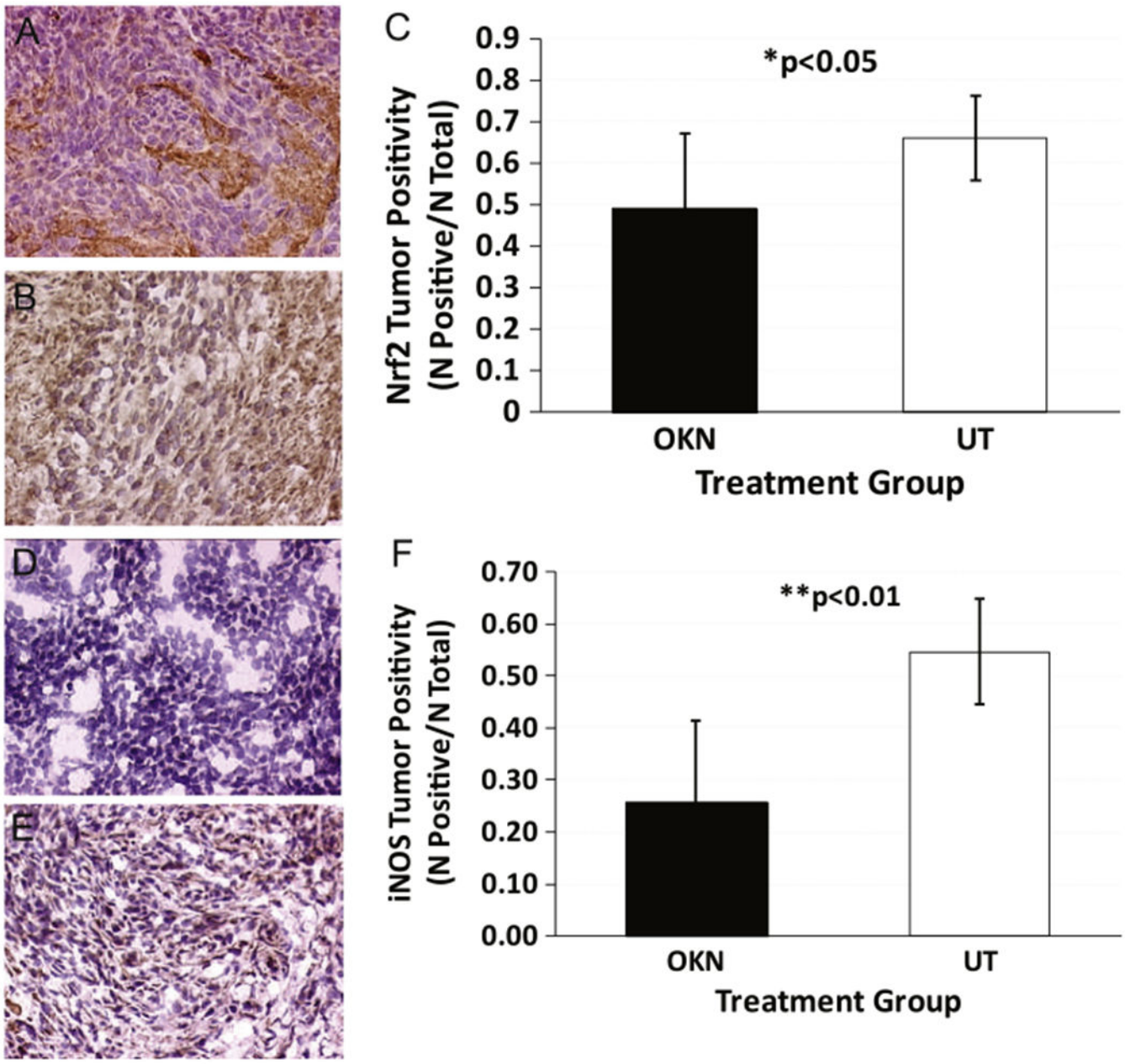


**Fig. 6.**

*Ex vivo* immunohistochemistry detection of Nrf2 and iNOS in F98 gliomas. IHC detection of Nrf2 in OKN-007-treated and untreated (UT) F98 rat gliomas (central tumor regions). (A) Representative Nrf2 expression in an OKN-007-treated F98 glioma. (B) Representative Nrf2 expression in a UT F98 glioma. (C) Nrf2 tumor positivity (total of positive cells/total cells) in OKN-007-treated ($n$=5) and UT ($n$=9) F98 glioma tissues. There was a significant decrease in Nrf2 levels from OKN-007-treated tissues ($P$ = 0.0335) compared to UT samples. IHC detection of iNOS in OKN-007-treated ($n$=5) and untreated (UT) ($n$=8) F98 rat gliomas (central tumor regions). (D) Representative iNOS expression in an OKN-007-treated F98 glioma. (E) Representative iNOS expression in a UT F98 glioma. (F) iNOS

tumor positivity (total of positive cells/total cells) in OKN-007-treated and UT F98 glioma tissues. There was a significant decrease in iNOS levels from OKN-007-treated tissues ($P = 0.0018$) compared to UT samples.

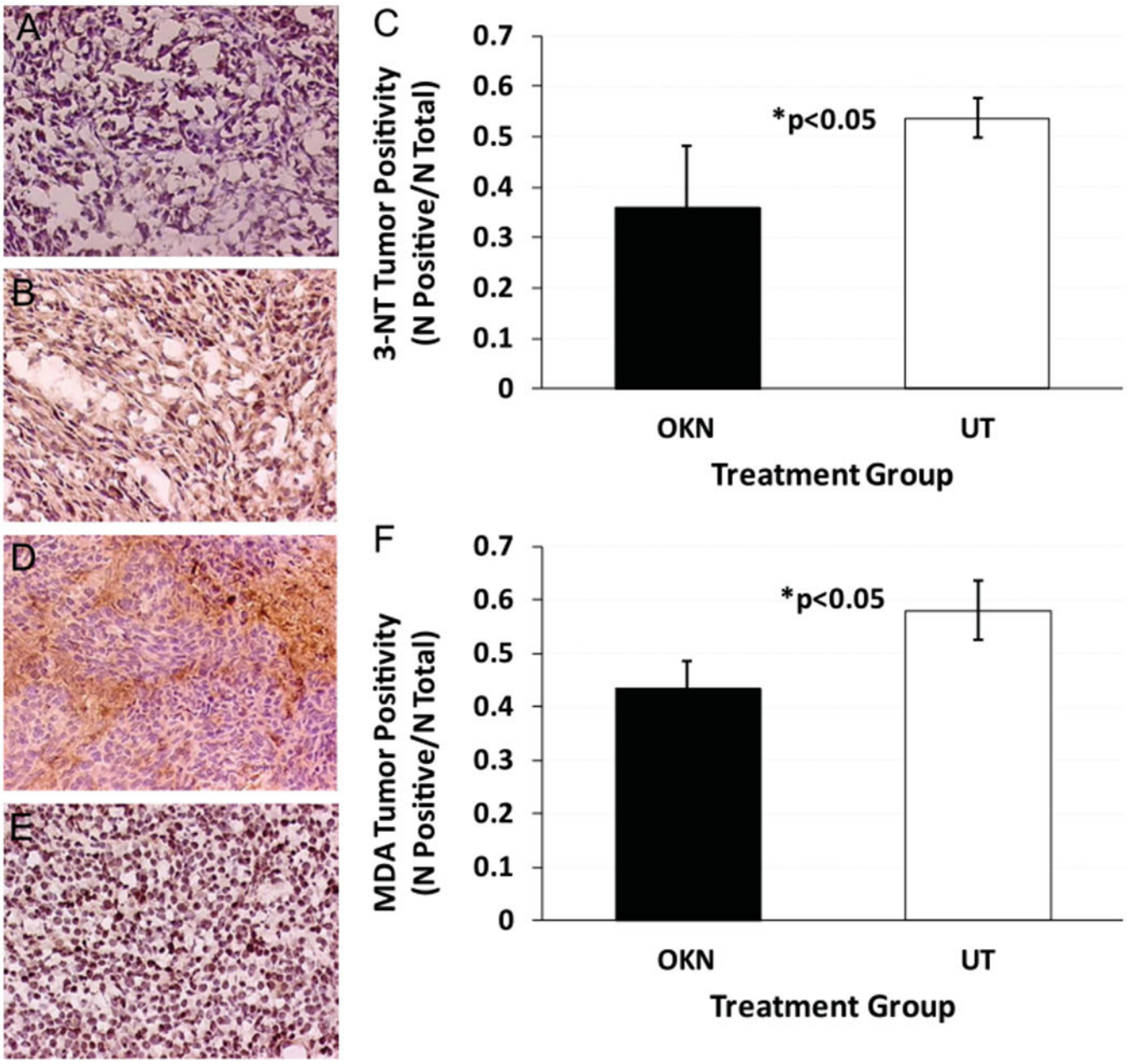


**Fig. 7.**

*Ex vivo* immunohistochemistry detection of 3-NT and MDA in F98 gliomas. IHC detection of 3-NT in OKN-007-treated and untreated (UT) F98 rat gliomas (central tumor regions). (A) Representative 3-NT expression in an OKN-007-treated F98 glioma. (B) Representative 3-NT expression in a UT F98 glioma. (C) 3-NT tumor positivity (total of positive cells/total cells) in OKN-007-treated ($n$=4) and UT ($n$=4) F98 glioma tissues. There was a significant decrease in 3-NT levels from OKN-007-treated tissues ($P$ = 0.0375) compared to UT samples. IHC detection of MDA protein adducts in OKN-007-treated, and untreated (UT) F98 rat gliomas (central tumor regions). (D) Representative MDA adduct expression in an OKN-007-treated F98 glioma. (E) Representative MDA adduct expression in a UT F98

glioma. (F) MDA adduct tumor positivity (total of positive cells/total cells) in OKN-007-treated ($n$=4) and UT ($n$=4) F98 glioma tissues. There was a significant decrease in MDA adduct levels from OKN-007-treated tissues ($P$ = 0.0154) compared to UT samples.

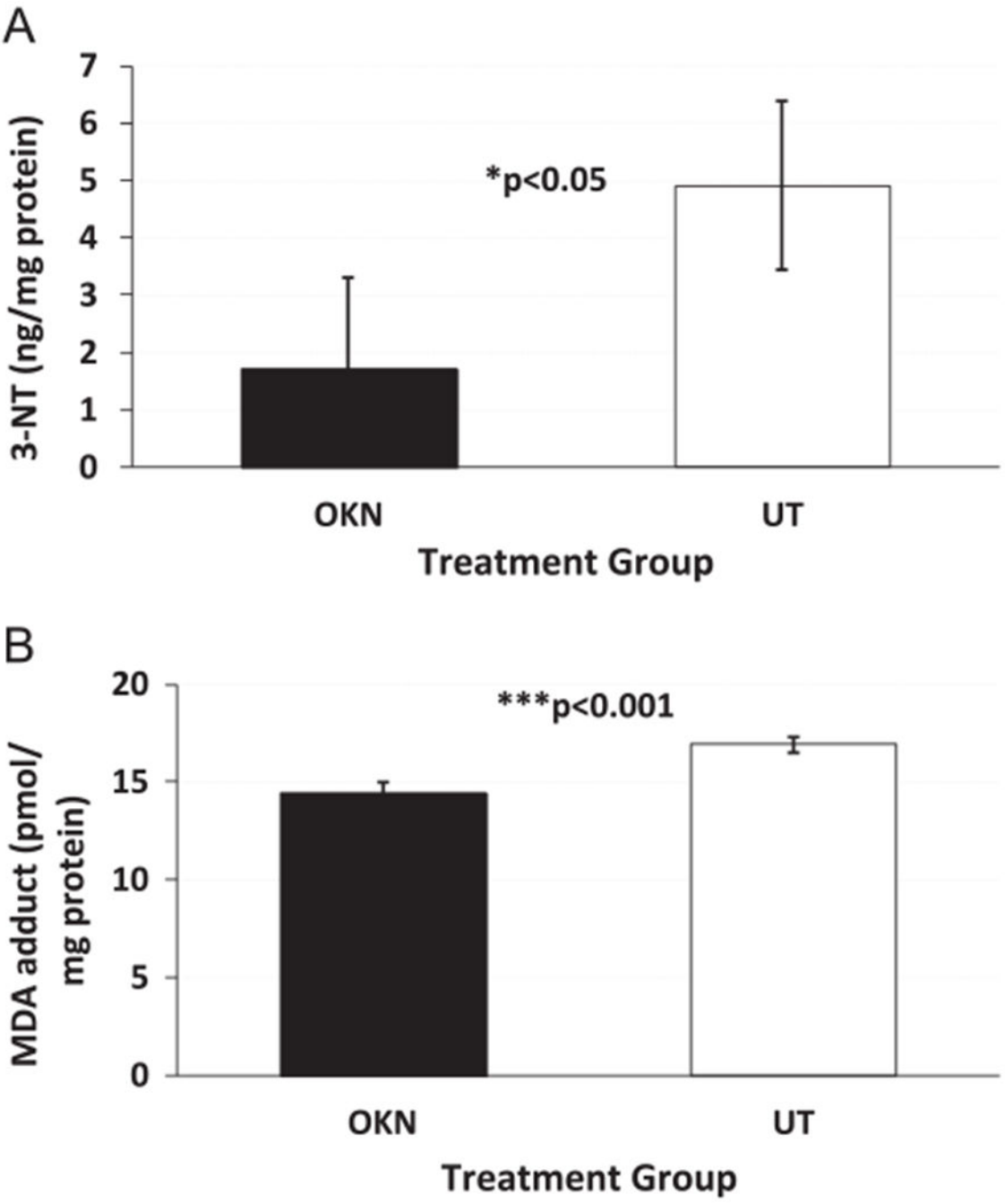


**Fig. 8.**

*In vitro* ELISA detection of 3-NT and MDA adducts in F98 glioma cells. (A) Detection of 3-NT in OKN-007-treated ($n$=4) and UT ($n$=4) F98 cells, both exposed to $H_2O_2$. There was a significant decrease in 3-NT levels following OKN-007 treatment ($P$ = 0.0264) compared to UT F98 cells. (B) Detection of MDA adducts in OKN-007-treated ($n$=4) and UT ($n$=4) F98 cells, both exposed to $H_2O_2$. There was a significant decrease in MDA adduct levels following OKN-007 treatment ($P$ = 0.0004) compared to UT F98 cells.

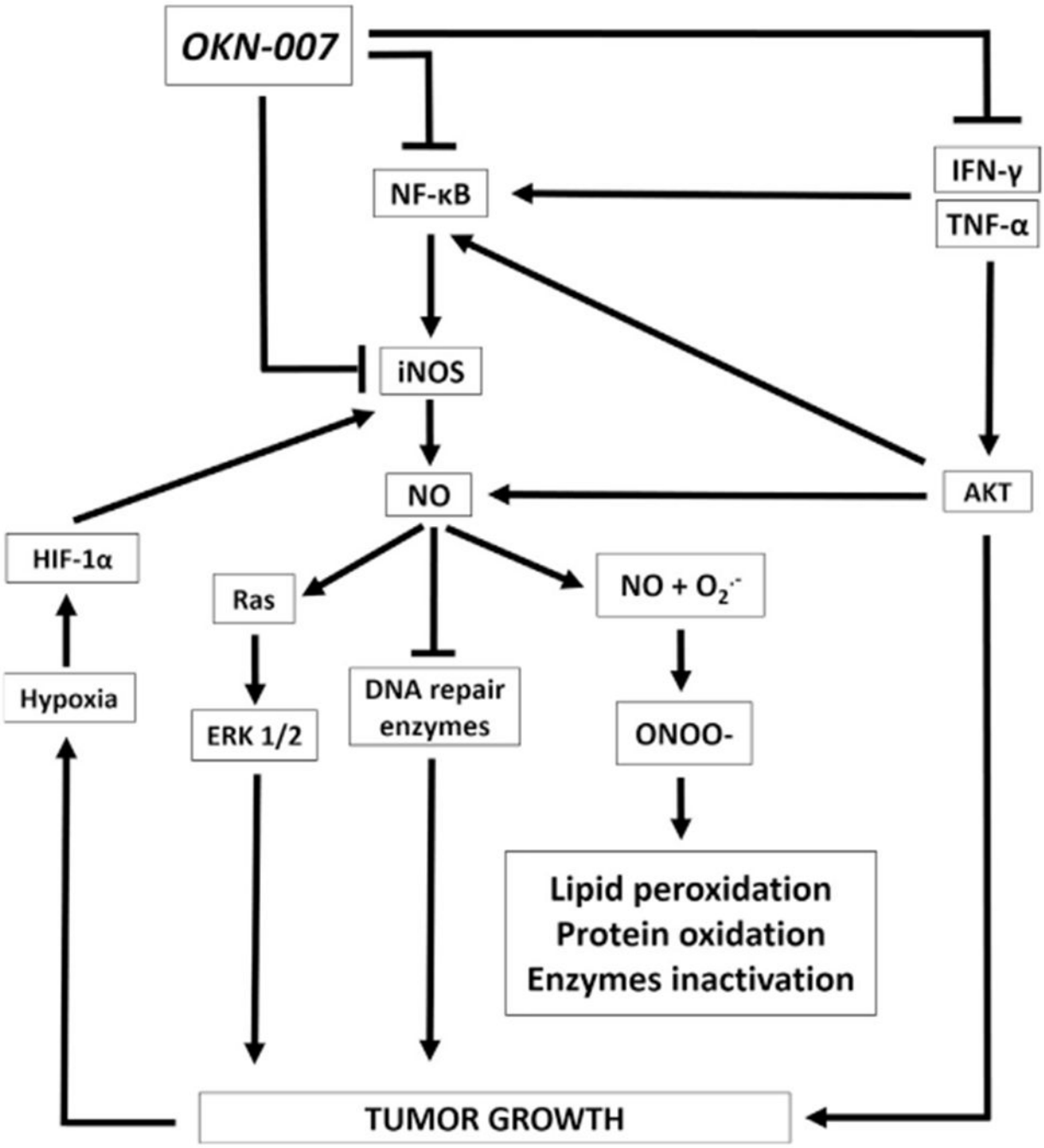


**Fig. 9.**

Schematic representation of possible antioxidant mechanisms of action for the anticancer agent OKN-007. OKN-007 scavenges radicals associated with tumor (e.g., glioma) growth. OKN-007 decreases iNOS (inducible nitric oxide synthase) activity and also downregulates some proinflammatory cytokines (TNF-α and IFN-γ) and NF-κB expression, which promotes iNOS expression and NO formation. ERK 1/2, extracellular signal-regulated kinase 1/2; HIF-1α, hypoxia inducible factor-1α; IFN-γ, interferon-gamma; iNOS,

inducible nitric oxide synthase; NO, nitric oxide; $ONOO^{-}$, peroxynitrite; $O_2^{\cdot -}$, superoxide anion, TNF-α, tumor necrosis factor alpha.